

Coupled oscillation model of spherical bubble cluster in liquid cavity wrapped by elastic shell

Xin-Yi Zuo(左馨怡), Rui Liu(刘睿), Zhao-Kang Lei(雷照康), Yu-Ting Wu(吴玉婷), Xiu-Ru Li(李秀如), and Cheng-Hui Wang(王成会)

Citation: Chin. Phys. B, 2025, 34 (**10**): 104302. DOI: 10.1088/1674-1056/addce7
http://cpb.iphy.ac.cn; http://iopscience.iop.org/cpb

What follows is a list of articles you may be interested in

Acoustic radiation force on a cylindrical composite particle with an elastic thin shell and an internal eccentric liquid column in a plane ultrasonic wave field

Rui-Qi Pan(潘瑞琪), Zhi-Wei Du(杜芷玮), Cheng-Hui Wang(王成会), Jing Hu(胡静), and Run-Yang Mo(莫润阳)
Chin. Phys. B, 2024, 33 (**9**): 094302. DOI: 10.1088/1674-1056/ad5d66

Behaviors of cavitation bubbles driven by high-intensity ultrasound

Chen-Yang Huang(黄晨阳), Fan Li(李凡), Shi-Yi Feng(冯释毅), Cheng-Hui Wang(王成会), Shi Chen(陈时), Jing Hu(胡静), Xin-Rui He(何芯蕊), and Jia-Kai Song(宋家凯)
Chin. Phys. B, 2024, 33 (**2**): 024301. DOI: 10.1088/1674-1056/ad0717

Effects of adjacent bubble on spatiotemporal evolutions of mechanical stresses surrounding bubbles oscillating in tissues

Qing-Qin Zou(邹青钦), Shuang Lei(雷双), Zhang-Yong Li(李章勇), and Dui Qin(秦对)
Chin. Phys. B, 2023, 32 (**1**): 014302. DOI: 10.1088/1674-1056/ac70ba

Acoustic radiation force on thin elastic shells in liquid

Run-Yang Mo(莫润阳), Jing Hu(胡静), Shi Chen(陈时), Cheng-Hui Wang(王成会)
Chin. Phys. B, 2020, 29 (**9**): 094301. DOI: 10.1088/1674-1056/ab943e

Interaction of a bubble and a bubble cluster in an ultrasonic field

Wang Cheng-Hui (王成会), Cheng Jian-Chun (程建春)
Chin. Phys. B, 2013, 22 (**1**): 014304. DOI: 10.1088/1674-1056/22/1/014304

Coupled oscillation model of spherical bubble cluster in liquid cavity wrapped by elastic shell

Xin-Yi Zuo(左馨怡), Rui Liu(刘睿), Zhao-Kang Lei(雷照康),
Yu-Ting Wu(吴玉婷), Xiu-Ru Li(李秀如), and Cheng-Hui Wang(王成会)†

Institute of Shaanxi Key Laboratory of Ultrasonics, Shaanxi Normal University, Xi'an 710119, *China*

(Received 9 April 2025; revised manuscript received 26 May 2025; accepted manuscript online 27 May 2025)

Bubbles within an elastic shell, which undergo ultrasound-driven oscillation to treat tumors and soft tissues, are frequently treated as viscoelastic media. Therefore, studying the dynamic behavior of bubbles wrapped in a viscoelastic medium while considering an elastic shell can provide theoretical support for ultrasound biotherapy. Bubbles are always in the form of clusters. Therefore, a model of spherical bubble clusters in a liquid cavity wrapped by an elastic shell was constructed, the coupled oscillation equations of bubbles were obtained by taking into account the dynamic effects of the elastic shell and the viscoelastic media outside the cavity, and the oscillation behaviors of the bubbles were analyzed. Acoustic waves at 1.5 MHz could cause bubbles with a radius of 1 μm to resonate. Increasing the number of bubbles increased the suppressing effect of bubble oscillation caused by bubble interaction. The bubble cluster oscillation caused the elastic shell to oscillate and be stressed, and the stress trend was the inverse of the bubble oscillation trend with maximal tensile and compressive stresses. Bubbles with an equilibrium radius of 2 μm exhibited the lowest inertial cavitation threshold, making inertial cavitation more likely under high-frequency acoustic excitation. The inertial cavitation threshold of bubbles was heavily influenced by the acoustic wave frequency, bubble number density, and bubble cluster radius. The nonspherical oscillation stability of bubbles was primarily affected by the driving acoustic pressure amplitude and frequency, bubble initial radius, bubble number density, and bubble cluster radius. The acoustic frequency and amplitude exhibited a synergistic effect, with a minimum unstable driving acoustic pressure threshold of approximately 0.13 MPa. The initial radius within the elastic shell affected the minimum unstable driving acoustic pressure threshold.

Keywords: spherical bubble cluster, elastic shell, cavitation bubbles, coupled oscillations

PACS: 43.35.+d, 43.25.+y, 47.55.dp

DOI: 10.1088/1674-1056/addce7 **CSTR:** 32038.14.CPB.addce7

1. Introduction

Ultrasound is rapidly developing in medicine, and the use of microbubbles as ultrasound contrast agents has improved the quality of medical imaging.[1] Studying the dynamic behavior of cavitating bubbles in a liquid cavity can provide theoretical and experimental support for cancer therapy and drug delivery.[2–9] Many bubbles are confined in nature. The xylem of plants is filled with liquid, and the growth of xylem bubbles during drought is thought to be responsible for the early death of plants from drought.[10] Ferns use bubbles to store elastic energy when dehydrating to power the ejection of spores,[11] and the confined bubbles can be used to calculate the soil tensile force.[12] The geometrical models of constrained bubble three-phase systems are classified as bubble–solid shell–liquid,[13] bubble–liquid–air,[14] bubble–liquid–solid shell,[15] and bubble–liquid–elastic solid,[16] with the bubble–liquid–elastic solid model receiving the most attention.

Cavitation can develop when ultrasound is applied to biological tissue, and the environment around the bubble can be represented as a viscoelastic medium. Vincent *et al.* observed rapid volumetric oscillations of bubbles in gels under negative pressure and abundant nonspherical dynamic behaviors.[17] They theoretically investigated the hydrostatics and dynamics of bubbles in fully confined liquids, derived equations controlling the dynamics of natural oscillations of fully enclosed bubbles, and found that the compressibility of the liquid and the elasticity of the walls cause rapid radial oscillations of bubbles.[16] Wang[18] found that for a single bubble in a liquid cavity wrapped by an elastic solid, the frequency of oscillation increases with respect to the bubble in the unbounded liquid and that the bubble takes longer to reach the steady state and has a larger equilibrium radius by numerical analysis. To simplify the analysis, bubbles in tissues are often assumed to be spherical, but nonspherical effects have a strong influence on the extent of tissue damage. Gaudron and Murakami *et al.*[19] derived dynamic equations for nonspherical perturbations on the surface of bubbles in two elasticity models using perturbation theory, investigated the shape stability, and found that the shape stability was enhanced when the shear modulus of the medium was increased. The three-phase system research serves as a theoretical foundation for bubble–internal liquid–elastic shell–external liquid four-phase systems. Acoustic droplets are now often used in gas embolism treatment as a bubble–internal liquid–elastic shell–external liquid four-phase

†Corresponding author. E-mail: wangld001@snnu.edu.cn

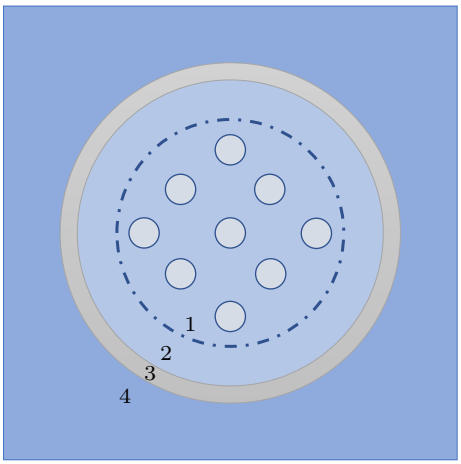
© 2025 Chinese Physical Society and IOP Publishing Ltd. All rights, including for text and data mining, AI training, and similar technologies, are reserved.

system owing to the development of novel materials. A theoretical examination of the vaporization process of acoustic droplets demonstrated that bubble growth is severely limited by high viscosity and surface tension for droplet diameters smaller than 6 μm.[20] Gubaidullin and Fedorov[21] derived the modified Rayleigh–Lamb equation, accounting for the radial oscillation of a droplet, and investigated the effect of shell viscoelasticity on acoustic dynamics. They found that the resonant frequency of the inclusions increases when the bubble has a viscoelastic shell.

Bubbles are usually in the form of bubble clusters,[22] and there are interactions between the bubbles; therefore, developing a bubble cluster model is required for a better understanding of the cavitation dynamics behavior of bubbles in tissues. An[23] established equations of multibubble motion in two cases: filament of bubbles and a small spherical cluster of bubbles. The numerical simulations showed that the interactions between bubbles suppressed the intensity of bubble oscillations, and the denser the distribution of bubbles, the stronger the interactions and the more obvious the suppression. Shen *et al.*[24] established a bubble dynamics model for viscoelastic media using the Keller–Miksis equation and the Kelvin–Voigt constitutive model, taking into account bubble–bubble interactions. They discovered that the effect of bubble clusters on bubble oscillation alternates with frequency and that the oscillation promotion effect is larger for bubbles with a radius of 10 μm. To analyze the coupled dynamic effects of tissue cavitation and elastic shell, we developed a coupled oscillation model of a spherical bubble cluster in a liquid cavity wrapped by an elastic shell, taking into account the interactions between bubbles, and predicted the oscillatory behavior of bubbles as well as the effects of cavitation in the bubble cluster system.

2. Model theory

To explore the dynamic behavior of bubbles within a confined liquid cavity bubble cluster, a simplified model of the spherical distribution of bubbles in a liquid cavity wrapped by an elastic shell within a viscoelastic medium, as shown in Fig. 1, was used to develop the theory of multibubble dynamics in a liquid cavity, taking into account the interactions between bubbles and the thickness of the elastic shell. Media 1, 2, 3, and 4 in the figure illustrate the bubble cluster, the liquid within the elastic shell, the elastic shell, and the liquid outside the elastic shell, respectively. The bubbles may undergo translational motion under ultrasound.[25] The bubbles in the cavity showed irregular distribution and different radii. A numerical analysis was performed for bubbles with different radii. At this time, the cavity system was not a strictly spherically symmetric model, and the solution required the use of three-dimensional equations, which required a large amount of computational resources. Mass exchange occurred inside and outside the bubble, affecting the bubble collapse state. The bubble collapse pressure increased instantly, resulting in rapid condensation of water vapor, removing energy and reducing the maximum temperature of the bubble. Bubble group boundary oscillation and heat conduction affected the acoustic field distribution.[26] To simplify the model, we made the following assumptions while considering only the impact of the bubbles on the acoustic field: 1) the spherical bubble cluster is at the center of the liquid cavity in the elastic shell; 2) the bubbles in the bubble cluster are uniformly distributed and have the same radius; 3) the liquid in the cavity is incompressible; 4) the exchange of mass inside and outside the bubbles in the bubble cluster is neglected; 5) the exchange of mass of the liquid at the boundary of the bubble cluster is neglected; 6) the bubbles in the bubble cluster oscillate almost in synchrony, and the effect of the acoustic radiation at the boundary of the bubble cluster is ignored on the boundary of the bubble cluster; 7) the heat transfer between the bubble and the liquid interface is not considered; and 8) only the radial oscillations of the bubbles are considered, whereas the translational motion of the bubbles is ignored.



1 Bubble cluster
2 Liquid inside the elastic shell
3 Elastic shell
4 Liquid outside the elastic shell

Fig. 1. Spherical bubble cluster in a liquid cavity wrapped by an elastic shell within a viscoelastic medium.

The fluid inside the cavity and the elastic shell are impermeable; hence, the velocity of the exterior of the bubble cluster in spherical coordinates at r is expressed as

$$u(r,t) = \frac{r_c^2(t)}{r^2}\dot{r}_c(t), \tag{1}$$

where r_c is the bubble cluster radius, and $\dot{r}_c$ is the bubble cluster boundary oscillation velocity.

According to the momentum equation

$$\rho\left(\frac{\partial u}{\partial t} + u\frac{\partial u}{\partial r}\right) = -\frac{\partial p}{\partial r} + \frac{1}{r^2}\frac{\partial}{\partial r}(r^2\tau_{rr}) - \frac{\tau_{\theta\theta}+\tau_{\varphi\varphi}}{r}, \tag{2}$$

where ρ is the density, p is the pressure, and τ_{rr}, $\tau_{\theta\theta}$, and $\tau_{\varphi\varphi}$ are the stress components that fulfill the equation[27] $\tau_{rr} = -(\tau_{\theta\theta} + \tau_{\varphi\varphi})$. Integrating r from r_c to infinity yields

$$\begin{aligned}
&\left(2r_c\dot{r}_c^2 + r_c^2\ddot{r}_c\right)\left[\rho_l\left(\frac{1}{r_c} - \frac{1}{R_1}\right) + \rho_s\left(\frac{1}{R_1} - \frac{1}{R_2}\right) + \rho_e\frac{1}{R_2}\right] \\
&+ \frac{r_c^4\dot{r}_c^2}{2}\left[\rho_l\left(\frac{1}{R_1^4} - \frac{1}{r_c^4}\right) + \rho_s\left(\frac{1}{R_2^4} - \frac{1}{R_1^4}\right) - \rho_e\frac{1}{R_2^4}\right] \\
&= p_c - p_l(R_1,t) - p_s(R_2,t) + p_s(R_1,t) - p_\infty + p_l(R_2,t) \\
&+ 3\int_{r_c}^{R_1}\frac{\tau_{rr,l}}{r}\,\mathrm{d}r + 3\int_{R_1}^{R_2}\frac{\tau_{rr,s}}{r}\,\mathrm{d}r \\
&+ 3\int_{R_2}^{\infty}\frac{\tau_{rr,e}}{r}\,\mathrm{d}r + \tau_{rr,l}(R_1,t) \\
&- \tau_{rr,l}(r_c,t) + \tau_{rr,s}(R_2,t) - \tau_{rr,s}(R_1,t) - \tau_{rr,e}(R_2,t), \qquad (3)
\end{aligned}$$

where $\ddot{r}_c$ is the acceleration of oscillation at the border of the bubble cluster, ρ_l is the internal liquid density, ρ_s is the density of the elastic shell, ρ_e is the density of the exterior liquid, and R_1 and R_2 are the radii of the elastic shell. Here, $p_\infty = p_0 + p_a\sin(2\pi ft)$, where f and p_a are the frequency and amplitude of the driving acoustic wave, respectively; p_c is the liquid pressure inside the bubble cluster; p_l and p_s are the liquid pressure and elastic shell pressure, respectively; and the subscripts l, s, and e of τ represent the internal liquid elastic shell, elastic shell, and external liquid, respectively. Considering the presence of surface tension, the boundary equation between the media is

$$p_s(R_1,t) - p_l(R_1,t) + \frac{2\sigma_1}{R_1} = \tau_{rr,s}(R_1,t) - \tau_{rr,l}(R_1,t), \qquad (4)$$

$$p_l(R_2,t) - p_s(R_2,t) + \frac{2\sigma_2}{R_2} = \tau_{rr,l}(R_2,t) - \tau_{rr,s}(R_2,t), \qquad (5)$$

where σ_1 and σ_2 are the surface tension coefficients of the inner and outer elastic shells, respectively. Simplification yields

$$\begin{aligned}
&\left(2r_c\dot{r}_c^2 + r_c^2\ddot{r}_c\right)\left[\rho_l\left(\frac{1}{r_c} - \frac{1}{R_1} + \frac{1}{R_2}\right) + \rho_s\left(\frac{1}{R_1} - \frac{1}{R_2}\right)\right] \\
&+ \frac{r_c^4\dot{r}_c^2}{2}\left[\rho_l\left(\frac{1}{R_1^4} - \frac{1}{r_c^4} - \frac{1}{R_2^4}\right) + \rho_s\left(\frac{1}{R_2^4} - \frac{1}{R_1^4}\right)\right] \\
&= p_c - p_\infty - \frac{\sigma_1}{R_1} - \frac{\sigma_2}{R_2} - \tau_{rr,l}(r_c,t) \\
&+ 3\int_{r_c}^{R_1}\frac{\tau_{rr,l}}{r}\,\mathrm{d}r + 3\int_{R_1}^{R_2}\frac{\tau_{rr,s}}{r}\,\mathrm{d}r + 3\int_{R_2}^{\infty}\frac{\tau_{rr,l}}{r}\,\mathrm{d}r, \qquad (6)
\end{aligned}$$

where

$$\tau_{rr,l}(r_c,t) = -4\left[\frac{G_l(r_c^3 - r_{c0}^3)}{3r_c^3} + \mu_l\frac{\dot{r}_c}{r_c}\right],$$

$$3\int_{r_c}^{R_1}\frac{\tau_{rr,l}}{r}\,\mathrm{d}r = \left[\frac{4G_l(r_c^3 - r_{c0}^3)}{3} + 4\mu_l r_c^2\dot{r}_c\right]\left(\frac{1}{R_1^3} - \frac{1}{r_c^3}\right),$$

$$3\int_{R_1}^{R_2}\frac{\tau_{rr,s}}{r}\,\mathrm{d}r = -\frac{4\mu_s}{R_1}\left(1 - \frac{R_1^3}{R_2^3}\right)\dot{R}_1 + Y,$$

$$\begin{aligned}
Y = G_s\Bigg[&(1+\beta)\left(\frac{R_{10}}{R_1} - \frac{R_{20}}{R_2} + \frac{R_{10}^4}{4R_1^4} - \frac{R_{20}^4}{4R_2^4}\right) \\
&+ (1-\beta)\left(\frac{R_2}{R_{20}} - \frac{R_1}{R_{10}} + \frac{R_{20}^2}{2R_2^2} + \frac{R_{10}^2}{4R_1^2}\right)\Bigg],
\end{aligned}$$

$$3\int_{R_2}^{\infty}\frac{\tau_{rr,e}}{r}\,\mathrm{d}r = -\frac{4G_e}{3}\left(1 - \frac{R_{20}^3}{R_2^3}\right) - \frac{4\mu_e R_1^2}{R_2^3}\dot{R}_1.$$

The shear moduli of the internal fluid, elastic shell, and exterior fluid are G_l, G_s, and G_e, respectively, whereas the viscosity coefficients of the internal fluid, elastic shell, and external fluid are μ_l, μ_s, and μ_e, respectively; β is a parameter that describes the stiffness of the shell material and was chosen as $\beta = 1$.[28] The initial radius of the bubble cluster is r_{c0}; the initial radii of the inner and outer elastic shells are R_{10} and R_{20}, respectively; the radii of the inner and outer elastic shells are R_1 and R_2, respectively; and the oscillation velocity at the inner border of elastic shell is $\dot{R}_1$.

Leaving aside the compressibility of the liquid in the cavity, the inner radius of the elastic shell and the radius of the bubble cluster are connected to the radius of the bubble:

$$R_1^3 = R_{10}^3 + \left(r_b^3 - r_{b0}^3\right)N, \qquad (7)$$

$$r_c^3 = r_{c0}^3 + \left(r_b^3 - r_{b0}^3\right)N, \qquad (8)$$

where r_{c0} and r_{b0} are the initial radii of the bubble cluster and bubble, respectively.

According to Ref. [23], the equation of bubble dynamics within a bubble cluster can be determined by examining the interactions between the bubbles:

$$\begin{aligned}
&\left(1 - M + \frac{3}{2}M_0\right)r_b\ddot{r}_b + \frac{3}{2}\left(1 - \frac{M}{3} + 2M_0\right)\dot{r}_b^2 \\
&= (1+M)\frac{1}{\rho_l}(p_b - p_c) + \frac{t_R}{\rho_l}\dot{p}_b, \qquad (9)
\end{aligned}$$

where $M = \dot{r}_b/c$ is the bubble wall Mach number; r_b is the bubble radius; $\dot{r}_b$ and $\ddot{r}_b$ are the radial velocity and acceleration of the bubble boundary, respectively; c is the speed of sound in the liquid; $t_R = r_b/c$ is the ratio of the bubble radius to the speed of sound; r_0 is the position of the bubble in the bubble cluster; $M_0 = N\frac{r_b}{r_c}\left(1 - \frac{r_0^2}{3r_c^2}\right)$ is a term established to take into consideration inter-bubble interactions, with various M_0 representing bubbles at different places inside the bubble cluster.[23] Assuming that all the bubbles are at the center of the liquid cavity; therefore, $r_0 = 0$. $p_b = p_g - \frac{2\sigma}{r_b} - 4\eta\frac{\dot{r}_b}{r_b}$ is the scattering pressure of the bubble, where $p_g = \left(p_0 + \frac{2\sigma}{r_{b0}}\right)\left(\frac{r_{b0}^3 - h^3}{r_b^3 - h^3}\right)^\kappa$ is the gas pressure inside the bubble. The joint equations (6) and (9) yield a set of equations describing the dynamics of spherical bubble clusters in a liquid cavity wrapped by an elastic shell with inter-bubble interactions.

As R_1 and R_2 tend to infinity, $3\int_{R_1}^{R_2}\frac{\tau_{rr,s}}{r}\mathrm{d}r$, $3\int_{R_1}^{R_2}\frac{\tau_{rr,s}}{r}\mathrm{d}r$, $\frac{\sigma_1}{R_1}$, $\frac{\sigma_2}{R_2}$, and $-\tau_{rr,l}(r_c,t) + 3\int_{r_c}^{R_1}\frac{\tau_{rr,l}}{r}\mathrm{d}r$ tend to zero. Equations (6) and (9) degenerate into dynamic equations for bubbles within a cluster of bubbles in an indefinitely large liquid[29] after removing p_c from the equation.

3. Numerical analysis and discussion

3.1. Comparison of models

To better understand the dynamic behavior of spherical bubble clusters wrapped by elastic shells while accounting for inter-bubble interactions, coupled equations (6) and (9) were solved using the Runge–Kutta method, and the numerical results were analyzed to predict the bubble dynamic behavior. Unless otherwise indicated, the liquid in the elastic shell exhibited the same characteristics as water: $\rho_{\mathrm{l}} = 1000\ \mathrm{kg/m^3}$, $\mu_{\mathrm{l}} = 0.001\ \mathrm{Pa\cdot s}$, $\sigma_{\mathrm{l}} = 0.07\ \mathrm{N/m}$, $G_{\mathrm{l}} = 0\ \mathrm{MPa}$, and $c_{\mathrm{l}} = 1500\ \mathrm{m/s}$. The elastic shell parameters were based on existing literature:[30] $\rho_{\mathrm{s}} = 1500\ \mathrm{kg/m^3}$, $\mu_{\mathrm{s}} = 0.1\ \mathrm{Pa\cdot s}$, $\sigma_1 = 0.042\ \mathrm{N/m}$, $\sigma_2 = 0.051\ \mathrm{N/m}$, and $G_{\mathrm{s}} = 200\ \mathrm{MPa}$. Soft tissue parameters were used for the liquid outside the elastic shell:[31] $\rho_{\mathrm{e}} = 1060\ \mathrm{kg/m^3}$, $\mu_{\mathrm{e}} = 0.015\ \mathrm{Pa\cdot s}$, $\sigma_{\mathrm{e}} = 0.056\ \mathrm{N/m}$, and $G_{\mathrm{e}} = 0.2\ \mathrm{MPa}$.

Under the same computational conditions, we used the parameters from the literature:[29] $f = 20\ \mathrm{kHz}$, $p_0 = 0.1\ \mathrm{MPa}$, $p_{\mathrm{a}} = 1.5p_0$, $N = 300$, $r_{\mathrm{b0}} = 5\ \mu\mathrm{m}$, $r_{\mathrm{c0}} = 1\ \mathrm{mm}$, $R_{10} = 1.5\ \mathrm{mm}$, and $r_{\mathrm{s0}} = 0.01\ \mu\mathrm{m}$. Coupled equations (6) and (9) were used to perform a dynamic analysis (model 1) of the coupled oscillations of bubbles within an elastic shell, and the results were compared with the coupled oscillation equations of spherical bubble cluster (model 2) by Wang *et al.*[29] As shown in Fig. 2(a), the horizontal coordinate T is the time period. The differences between the two models were minor, with the inclusion of the elastic shell resulting in a modest reduction in the maximum radius of the bubble, mostly in the form of a decrease in the maximum dimensionless radius of the bubble from 5.206 (model 2) to 5.198 (model 1).

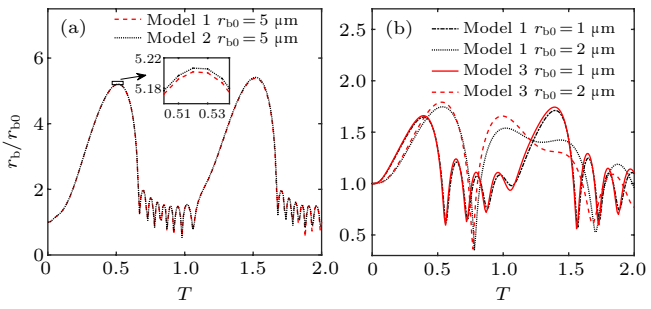


Fig. 2. Comparison (a) between the model in this study (model 1) and the infinite liquid vesicle group model (model 2), and (b) between the model in this study (model 1) and the elastic shell wrapped single bubble model (model 3).

By setting $f = 1\ \mathrm{MHz}$, $p_{\mathrm{a}} = 1.5p_0$, $N = 1$, $r_{\mathrm{c0}} = 50\ \mu\mathrm{m}$, $R_{10} = 200\ \mu\mathrm{m}$, and $r_{\mathrm{s0}} = 0.01\ \mu\mathrm{m}$, the model in this study was compared with the model of single bubble cavitation in a liquid cavity wrapped by an elastic shell (model 3) proposed in the literature,[21] as shown in Fig. 2(b). Both models exhibited significant nonlinearity at an initial bubble radius of 2 μm. The reason for this discrepancy may be the presence of bubble cluster constraints in the numerical calculations of model 1 compared to model 3, which slightly reduced the maximum dimensionless radius of the bubble. At an initial bubble radius of 1 μm, there was a minimal difference between the maximum dimensionless radius and bubble collapse time of the two models, which demonstrates the accuracy of the models in this study.

3.2. Characterization of bubble oscillations

By setting the driving acoustic wave amplitude as p_0, $1.2p_0$, $1.4p_0$, $r_{\mathrm{b0}} = 1\ \mu\mathrm{m}$, $N = 10$, $r_{\mathrm{c0}} = 30\ \mu\mathrm{m}$, $R_{10} = 60\ \mu\mathrm{m}$, and $r_{\mathrm{s0}} = 0.01\ \mu\mathrm{m}$, the oscillation curves of the maximum dimensionless radius of the bubble with the acoustic wave frequency were obtained, as shown in Fig. 3(a). The maximum dimensionless radius of the bubble fluctuated with the driving frequency, and there were individual protrusion spots, which might be due to the resonance of the bubble system under this circumstance, causing the maximum radius to increase. When the amplitude of the acoustic wave was p_0, the curve changed more softly in the low-frequency band. As the amplitude of the acoustic wave increased, the curve appeared to have an evidently large value, indicating that the bubble oscillation was significantly enhanced. The frequency corresponding to the maximum value was shifted to the low-frequency direction, indicating that the resonance frequency of the bubble varied with the amplitude of the driving acoustic wave.[32] Within this parameter, the resonance frequency of the bubble decreased as the acoustic wave amplitude increased.

With the driving acoustic wave amplitudes set (p_0, $1.2p_0$, and $1.4p_0$), the acoustic wave frequency set to $f = 1\ \mathrm{MHz}$, and all other parameters held constant, the maximum dimensionless radius of the bubble within the initial radius range of 0.5–10 μm changed with the initial radius, as shown in Fig. 3(b). When the initial radius of the bubble was less than 4 μm, the oscillation was more complicated, there were more resonance peaks at the maximum dimensionless radius, and there was a main resonance peak near 2 μm, which may be related to the resonance characteristics of the bubble and elastic shell system. The main resonance peak increased and shifted to the left with an increase in the driving acoustic amplitude, indicating an increase in the driving acoustic amplitude. When the initial radius of the bubble exceeded 4 μm, the driving acoustic wave amplitude exhibited little influence on the maximum dimensionless radius of the bubble, which tended to be close to 1 as the initial radius of the bubble increased.

The maximum dimensionless radius variation curves of the bubbles were obtained by setting the driving acoustic wave amplitude to p_0, $1.2p_0$, and $1.4p_0$; $f = 1\ \mathrm{MHz}$; $r_{\mathrm{b0}} = 1\ \mu\mathrm{m}$; the number of bubbles to 10–1000; and all other parameters constant (Fig. 3(c)). In the range of bubble numbers less than 300, the curve changes became more complicated, with distinct peaks in the bubbles at bubble numbers 200 and 60 and

a shift to the left as the driving acoustic wave increased. For more than 300 bubbles, the maximum radius of each bubble decreased as the number of bubbles increased.

To better understand the effects of the driving acoustic wave frequency, initial radius of bubbles, and number of bubbles on the maximum radius of the bubbles, the acoustic wave amplitude was set to 0.08–0.2 MPa, and the driving acoustic wave frequency, initial radius of bubbles, and number of bubbles ranged from 0.5 MHz to 2 MHz, 0.5 μm to 10 μm, and 10 to 1000, respectively, as shown in Figs. 3(d)–3(f). Each parameter was varied by keeping the rest constant. It was found that when the driving acoustic wave amplitude was less than 0.1 MPa, changing the frequency had a minimal effect on the maximum dimensionless radius of the bubble. In addition, low frequency had a smaller effect on the maximum radius than high frequency. With the increase in the acoustic wave amplitude, the effect of the frequency became increasingly significant, particularly when the driving acoustic wave amplitude was greater than 0.1 MPa, which changed the frequency of the maximum radius of the bubble. This result is similar to that shown in Fig. 3(a). At an initial bubble radius greater than 4 μm, the maximum radius of the bubble remained almost constant by altering the amplitude of the driving acoustic wave. When the initial radius of the bubble was less than 4 μm, the driving acoustic wave amplitude had a greater impact on its maximum radius, and as the driving acoustic wave amplitude increased, it also affected the bubble radius. When the driving acoustic wave amplitude remained constant and the initial radius of the bubble was changed, the maximum radius of the bubble occurred near 2 μm. The larger the driving acoustic wave amplitude, the smaller the corresponding initial radius, which is consistent with the results shown in Fig. 3(b). The effect of the number of bubbles on their maximum radius became significant as the driving acoustic wave increased. When the amplitude of the acoustic wave was greater than, the maximum radius of the bubbles varied with the number of bubbles, which is consistent with the conclusion obtained by Shen *et al.*[24] The inhibiting impact on bubbles becomes stronger as the number of bubbles increases, as represented by the lowering of the maximum radius that may be attained by bubble oscillation. The maximum radius reached its maximum value at 200 bubbles, which is consistent with the results presented in Fig. 3(c). The somewhat greater bubble radius at the bright spot parameter in Figs. 3(d)–3(f) might be the result of resonance.

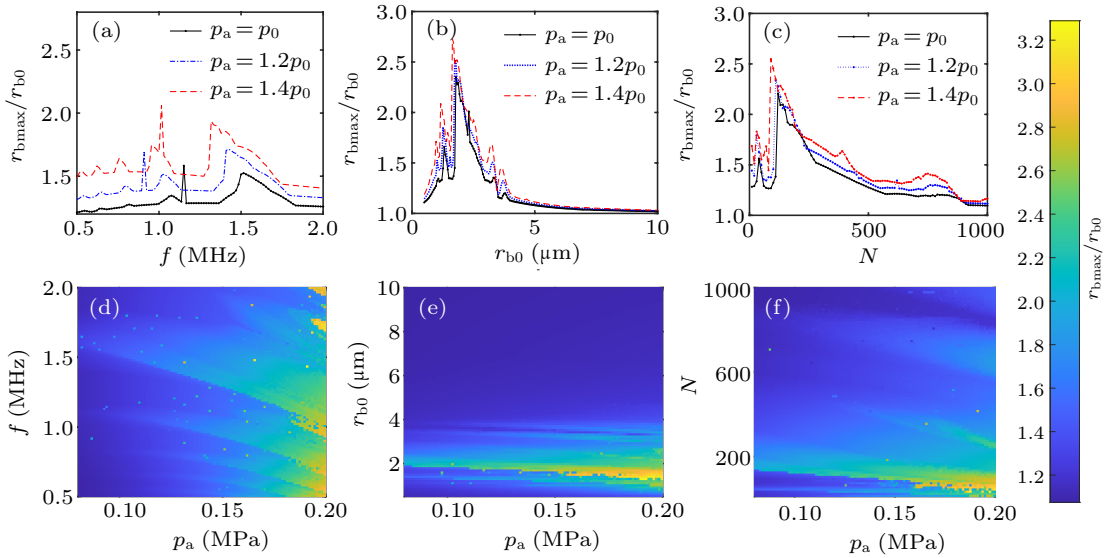


Fig. 3. The maximum dimensionless radius of bubbles as a function of (a) frequency, (b) initial radius of the bubble, and (c) bubble number. Bubble maximum dimensionless radius response plots: (d) f–p_a, (e) r_{b0}–p_a, and (f) N–p_a.

Bubble oscillations create oscillatory deformation of the elastic shell, which generates stress. When the stress is too high, the elastic shell may rupture.[32] Analysis of the change in stress on the elastic shell assists in predicting the rupture. The Zener model describes the connection between the stress and strain in a viscoelastic medium,[33] and the stress on the inner side of the elastic shell can be calculated using the following differential equation:

$$\tau_{rr} + \lambda_1 \dot{\tau}_{rr} = -\frac{4G_s}{3}\left(1 - \frac{R_{10}^3}{R_1^3}\right) - \frac{4\mu_s R_1^2 \dot{R}_1}{R_1^3}, \qquad (10)$$

where λ_1 is the relaxation time of the surrounding medium. The Zener model must satisfy $\lambda_1 < \mu_s/G_s$, which may be represented as $\lambda_1 = 10^{-11}$ s.

We set the frequency of the acoustic wave to 1 and 0.5 MHz, the amplitude to $1.5p_0$ and $2p_0$, and the initial radius of the bubble to 1 μm. The other parameters remained unchanged in the case of the oscillation curve of the bubble and stress curve, as shown in Fig. 4, where the stress was greater than zero for tensile stress and less than zero for compressive stress. A comparison of Figs. 4(a), 4(b) and 4(c), 4(d)

shows that increasing the amplitude of the acoustic wave increased both compressive and tensile loads on the elastic shell, as well as the maximum radius that the bubbles reached. Figures 4(a), 4(c), 4(b), and 4(d) show that when the frequency of the driving acoustic wave decreased, the compressive and tensile loads on the elastic shell and the maximum radius that may be attained also decreased significantly. The maximum tensile stress of the elastic shell occurred during the collapse phase of the bubble, whereas the maximum compressive stress occurred at the maximum radius of the bubble. The change in stress was opposite to the trend of the radius of the bubble. Therefore, the trend of the maximum dimensionless radius of the calculated bubble (Fig. 3) can be used to predict the trend of the maximum compressive stress. During ultrasound, perfluorocarbon droplets (four-phase system) were injected into the blood arteries that support cancer cells, causing bubbles to develop within the droplets and obstruct the blood vessels. Without blood supply, cancer cells cannot grow or spread.[20] The critical allowed stress of the shell material is a crucial characteristic that determines when the shell breaks. The model presented in this study may be used to determine parameters, such as the suitable frequency and amplitude of the driving acoustic wave, thereby avoiding shell rupture and improving shell structural stability.

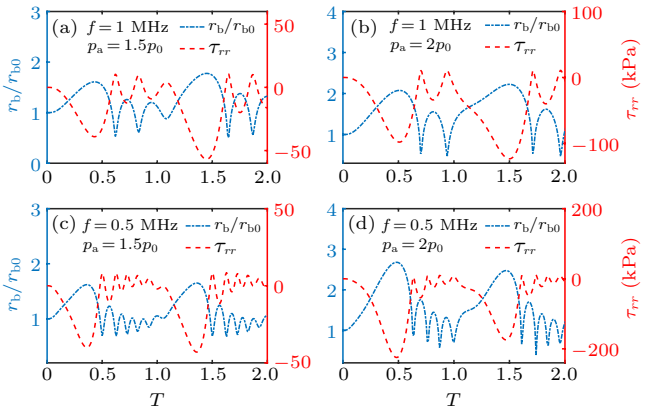


Fig. 4. Bubble oscillation curve and stress curve: (a) $f = 1$ MHz, $p_a = 1.5p_0$; (b) $f = 1$ MHz, $p_a = 2p_0$; (c) $f = 0.5$ MHz, $p_a = 1.5p_0$; (d) $f = 0.5$ MHz, $p_a = 2p_0$.

The change in the oscillation velocity of the bubble wall can also be a case of stress change, and the ratio of the oscillation velocity of the bubble wall to the speed of sound in the water is considered as the dimensionless oscillation velocity of the bubble wall. Figure 5 illustrates the fluctuation in the dimensionless oscillation velocity of the bubble wall with time for driving acoustic wave amplitudes of $p_a = 1.5p_0$ (Fig. 5(a)) and $p_a = 2p_0$ (Fig. 5(b)). When the driving acoustic wave frequency increased from $f = 0.5$ MHz to $f = 1$ MHz, the bubble collapsed and the rebound velocities increased. Comparing Figs. 5(a) and 5(b), it can be observed that the bubble collapsed and the rebound velocities increased with an increase in the driving acoustic wave amplitude, which is the same trend as the stress changes shown in Fig. 4, where the maximum collapse and rebound velocities correspond to the maximum tensile and compressive stresses, respectively.

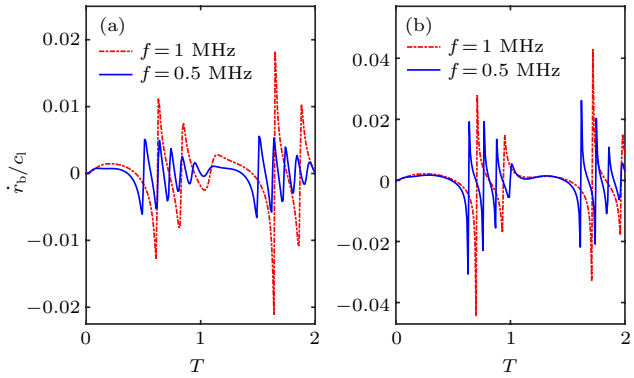


Fig. 5. The dimensionless oscillation velocity of the bubble wall as a function of time: (a) $p_a = 1.5p_0$ and (b) $p_a = 2p_0$.

3.3. Inertial cavitation threshold analysis

To study the cavitation behavior of bubbles in elastic shells, the acoustic wave amplitude that causes the maximum radius of oscillating bubbles to reach twice the initial radius was used as the inertial cavitation threshold to examine the effect of bubble cavitation.[34] By setting $f = 1$ MHz, $N = 10$, $r_{c0} = 30$ μm, $R_{10} = 60$ μm, we analyzed the bubbles with an initial radius range of 0.1–10 μm. Figure 6(a) shows the fluctuation of the bubble inertial cavitation thresholds with an initial radius by changing the thicknesses of the elastic shells to 0.01 μm, 0.1 μm, and 1 μm. When the initial radius of the bubble was less than 2 μm, the thickness of the elastic shell had little effect on the inertial cavitation threshold in this parameter range. The inertial cavitation threshold underwent a decreasing process in the range of 0.1–1 μm and then reached a flat zone after continuing to increase the initial radius of the bubble, with the lowest inertial cavitation threshold at approximately 2 μm, which was about 0.1 MPa. The very small points were around the initial radii of the bubble at 8 μm and 10 μm, whereas the significant difference in inertial cavitation thresholds could be attributed to the different elastic shell thicknesses and corresponding bubble initial radii of the bubble cluster, which formed a resonance system that reduced the inertial cavitation thresholds. When the initial bubble radius was larger than 6 μm, changing the initial radius of the inner elastic shell by 60 μm, 120 μm, and 180 μm (Fig. 6(b)) had a rather substantial influence on the inertial cavitation threshold of the bubble. As the cavity radius increased, the inertial cavitation threshold of the bubble decreased, and the bubble was more likely to experience inertial cavitation. There was little difference between the inner radii of the elastic shell of 120 μm and 180 μm, indicating that when the radius of the elastic shell is large, changing the radius of the elastic shell

has very little effect on the inertial cavitation threshold of the bubble.

With 5, 10, and 15 bubbles (Fig. 6(c)), an inner radius of the elastic shell of 60 μm, and other parameters remained unchanged, it was found that the inertial cavitation threshold was significantly affected by the number of bubbles when it was greater than 2 μm. The larger the number of bubbles, the higher the inertial cavitation threshold, probably because an increase in the number of bubbles increased the suppression of bubble oscillations, which led to an increase in the inertial cavitation threshold. When the number of bubbles reached 15, the inertial cavitation threshold tended to increase with increasing bubble radius at a large initial bubble radius. By setting the driving acoustic wave frequencies to 1 MHz, 2 MHz, and 3 MHz (Fig. 6(d)), the number of bubbles to 10, and all other parameters constant, it was found that the acoustic wave frequency had a substantial effect on the inertial cavitation threshold at values greater than 2 μm. The inertial cavitation threshold is strongly related to the acoustic frequency; the greater the acoustic frequency, the higher the inertial cavitation threshold and the more difficult it is for the bubble to experience inertial cavitation. We set the driving frequency to 1 MHz, the shear moduli of the external viscoelastic medium to 0.2 MPa, 2 MPa and 4 MPa, the viscosity coefficient to 0.015 Pa·s (Fig. 6(e)), the viscosity coefficients to 0.001 Pa·s, 0.015 Pa·s, and 0.1 Pa·s, and the shear modulus to 0.2 MPa (Fig. 6(f)). Each parameter was varied by keeping the rest constant. The shear modulus of the external viscoelastic medium and the viscosity coefficient were shown to have a substantial influence on the inertial cavitation threshold for a bubble with an initial radius larger than 4 μm.

We set the shear modulus and viscosity coefficient of the medium outside the cavity to 0.2 MPa and 0.015 Pa·s, respectively, and the radii of the bubble cluster to 30 μm, 40 μm, and 50 μm (Fig. 6(g)). When the initial radius of the bubble was greater than 4 μm, the radius of the bubble cluster significantly affected the inertial cavitation threshold of the bubble. The smaller the radius of the bubble cluster, the higher is the inertial cavitation threshold of the bubble, implying that the smaller the radius of the bubble cluster, the more difficult it is for the bubble to experience inertial cavitation. We set the radius of the bubble cluster to 30 μm, the shear moduli of the elastic shell to 200 MPa, 400 MPa, and 600 MPa, and the viscosity coefficient to 0.1 Pa·s (Fig. 6(h)). As shown in Fig. 6(i), the viscosity coefficients were 0.1 Pa·s, 5 Pa·s, and 10 Pa·s, and the shear modulus was 200 MPa. When the initial radius of the bubble was greater than 6 μm, the shear modulus of the elastic shell had a considerable influence on the inertial cavitation threshold. The larger the bubble radius, the greater was the difference at different shear moduli. The viscosity coefficient of the elastic shell had a minor influence on the inertial cavitation threshold of the bubbles, changing only around an initial bubble radius of 10 μm.

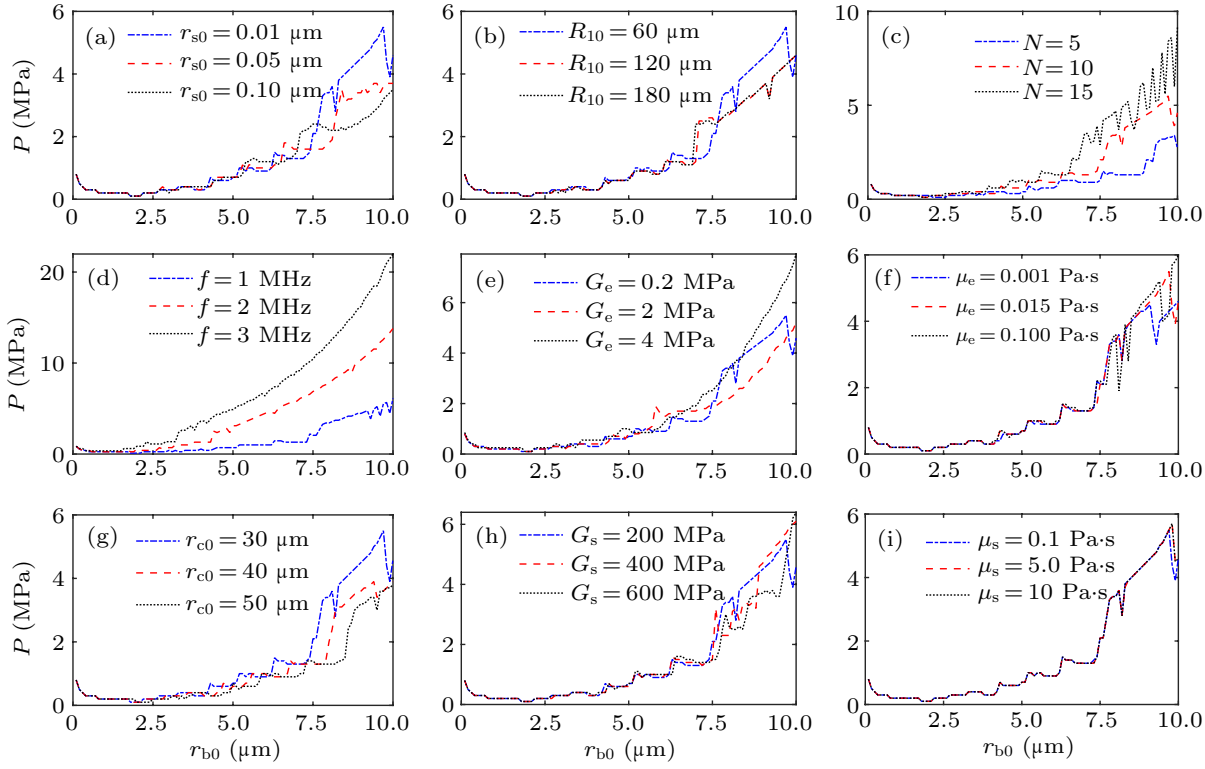


Fig. 6. Variation in inertial cavitation threshold with bubble initial radius under different conditions: (a) elastic shell thicknesses r_{s0}, (b) initial radius of the inner side of elastic shells R_1, (c) density of bubble number N, (d) acoustic frequencies f, (e) shear modulus of viscoelastic media G_e, (f) viscosity coefficients for viscoelastic media μ_e, (g) radius of bubble groups r_{c0}, (h) shear modulus of elastic shells G_s, and (i) viscosity coefficients of elastic shells μ_s.

3.4. Non-spherical stability analysis

Increasing the ambient pressure may cause the bubbles to lose their spherical shape, resulting in numerous bubbles and the creation of microjets.[35] When the spherical oscillations of a bubble are perturbed by nonspherical perturbations, the bubble may regain its spherical shape over time or deviate from its spherical shape and eventually collapse. The nth-order shape mode amplitude of a nonspherical bubble is represented as[36]

$$\ddot{a}_n(t) + B_n(t)\dot{a}_n(t) - A_n(t)a_n(t) = 0, \tag{11}$$

with

$$B_n = 3\frac{\dot{r}_\mathrm{b}}{r_\mathrm{b}} - 2(n+2)\left[(n-1)(n+1) - \frac{n(n+2)}{1+2\delta/r_\mathrm{b}}\right]\frac{\eta}{\rho r_\mathrm{b}^2}, \tag{12}$$

$$A_n = \frac{(n-1)}{r_\mathrm{b}}\left[\ddot{r}_\mathrm{b} - (n+1)(n+2)\frac{\sigma}{\rho r_\mathrm{b}^2} - 2(n+2)\left(n+1-\frac{n}{1+2\delta/r_\mathrm{b}}\right)\frac{\eta\dot{r}_\mathrm{b}}{\rho r_\mathrm{b}^2}\right], \tag{13}$$

$$\delta = \min\left(\sqrt{\frac{\eta}{f\rho}}, \frac{r_\mathrm{b}}{2n}\right), \tag{14}$$

where f is the frequency of the driving acoustic wave. To better judge the stability of the spherical oscillation of the bubble, the ratio of the nonspherical coefficient of the bubble to the initial radius of the bubble $a_n/r_{\mathrm{b}0}$ was used as the object of analysis. If $a_n/r_{\mathrm{b}0} < 1$, the bubble within the bubble cluster performs a stable nonspherical oscillation. If $a_n/r_{\mathrm{b}0} > 1$, the bubble within the bubble cluster performs an unstable nonspherical oscillation, and the bubble gradually collapses. The impact of second-order bubble surface oscillation modes on nonspherical oscillations is prominent;[36] hence, $n = 2$ was set in the analysis procedure. The parameters $f = 1$ MHz, $N = 10$, $r_{\mathrm{c}0} = 30$ μm, $R_{10} = 60$ μm, and $G_\mathrm{s} = 200$ MPa were set to assess the nonspherical stability of the bubble at its initial radius, and the results are shown in Fig. 7(a), where black represents the stable zone and white represents the unstable region. The unstable region is mainly distributed in the range where the initial radius of the bubble is less than 3 μm and the amplitude of the sound wave is greater than 0.1 MPa. The minimum unstable driving sound pressure thresholds corresponding to different initial radii are different, and decrease and then increase with an increase in the initial radius. A bubble with an initial radius of 1 μm corresponds to a minimum unstable driving sound pressure threshold of around 0.14 MPa. To investigate the influence of each parameter on the nonspherical stability of bubbles, bubbles with an initial radius of 1 μm were chosen for investigation, and the nonspherical response of bubbles with the number of bubbles set to 10–1000 and other parameters unaltered is shown in Fig. 7(b). Unstable regions were mostly created when the bubble number density was less than 200 and took the shape of scattered or linked sheets, whereas stable regions occurred only when the number of bubbles was considerable.

When the driving acoustic wave frequency was set to 0.02–2 MHz, $N = 10$, the other parameters were kept constant, and the nonspherical stability of the bubble was observed, it was found that the driving acoustic wave frequency had a significant effect on the minimum unstable driving acoustic pressure threshold of the bubble. The higher the frequency, the more significant the effect (Fig. 7(c)). The sound wave amplitude and frequency had a synergistic impact, with higher amplitudes separating the linear stable region from the unstable regions. When the radius of the bubble cluster was set to 10–50 μm, $R_{10} = 100$ μm, and the other parameters were kept constant (Fig. 7(d)), the radius of the bubble cluster significantly affected the minimum unstable driving acoustic pressure threshold of the bubble. The effect on the stability of the nonspherical shape was more complex when the acoustic wave amplitude was larger than that of the nonspherical shape. A curve-like stable region was observed within the unstable region. When the shear modulus G_e of the external viscoelastic medium was set to 0.1–5 MPa and the other parameters were kept constant (Fig. 7(e)), it was found that varying the shear modulus of the external viscoelastic medium outside the cavity had a greater effect on the nonspherical stability of the bubbles at high driving acoustic wave amplitudes. Arc-like stable regions were observed within the unstable regions. The nonspherical stability is shown in Fig. 7(f) when the starting radius of the inner side of the elastic shell was set to 0.05–1 mm, $f = 1$ MHz, and all other parameters were kept constant. The minimum unstable driving sound pressure threshold of the bubbles increased at a radius of less than 100 μm. The smaller the radius, the more significant the increase, which is most likely due to the smaller elastic shell having a stronger inhibitory effect on bubble oscillations, resulting in an increase in the minimum unstable driving sound pressure threshold. It was also found that changing the shear modulus G_s of the elastic shell, viscosity coefficient μ_s, elastic thickness $r_{\mathrm{s}0}$, and viscosity coefficient of the external viscoelastic medium μ_e had no influence on the nonspherical stability of the bubbles.

When the driving acoustic wave frequencies were set to 0.5 MHz and 2 MHz and the other parameters were set to $N = 10$, $r_{\mathrm{c}0} = 30$ μm, $R_{10} = 60$ μm, and $G_\mathrm{s} = 200$ MPa, the nonspherical stability of the bubbles with an initial radius of 0.5–10 μm was investigated, and the results are presented in Fig. 8. When compared with the driving acoustic frequency of 1 MHz (Fig. 7(a)), it was found that the higher the frequency, the smaller the corresponding unstable region in the $r_{\mathrm{b}0}$–p_a parameter plane. When the driving frequency was 2 MHz, the unstable region occurred only when the initial bubble radius was less than 2 μm. At the same time, the initial bubble radii were 2 μm and 3 μm, and other parameters were $N = 10$,

$r_{c0} = 30$ μm, $R_{10} = 60$ μm, $G_s = 200$ MPa, and driving acoustic frequency in the bubble of the nonspherical stability of the analysis, as shown in Fig. 9. In comparison with the initial bubble radius of 1 μm (Fig. 7(c)), it was found that the larger the initial bubble radius, the smaller the corresponding unstable region in the f–p_a parameter plane. The unstable region existed only when the driving acoustic wave frequency was less than 0.6 MHz when the initial bubble radius was 3 μm.

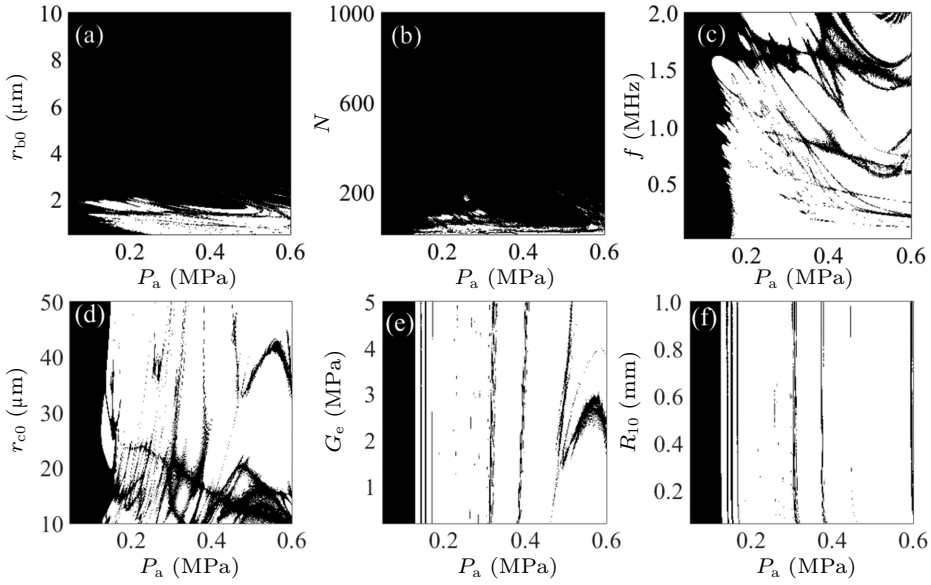


Fig. 7. Ratio of bubble nonspherical coefficient to bubble radius on different parameter planes: (a) r_{b0}–p_a, (b) N–p_a, (c) f–p_a, (d) r_{c0}–p_a, (e) G_e–p_a, and (f) R_{10}–p_a (black, stable; white, unstable).

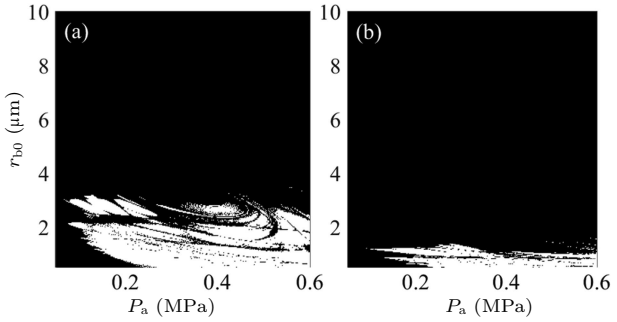


Fig. 8. Ratio of bubble nonspherical coefficient to bubble radius (a_n/r_{b0}) in the r_{b0}–p_a parameter plane at different driving frequencies: (a) $f = 0.5$ MHz and (b) $f = 2$ MHz (black, stable; white, unstable).

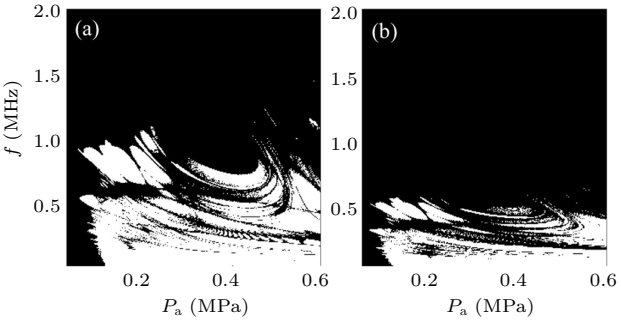


Fig. 9. Ratio of bubble nonspherical coefficient to bubble radius (a_n/r_{b0}) in the f–p_a parameter plane for different initial bubble radii: (a) $r_{b0} = 2$ μm and (b) $r_{b0} = 3$ μm (black, stable; white, unstable).

4. Conclusions

When using high-intensity ultrasonic stimulation of multibubble systems, coupling interactions between bubbles must be considered. In this study, we developed a connected oscillation model of a spherical bubble cluster in a liquid cavity wrapped by an elastic shell and a theoretical derivation of the model. The dynamic properties of the bubbles inside the bubble cluster and stress variations experienced by the elastic shell were investigated. To analyze the bubble oscillation instability and cavitation threshold, the influences of the initial radius of the bubbles, driving acoustic pressure amplitude and frequency, radius of the inner side of the elastic shell, radius of the bubble cluster, and shear modulus and viscosity coefficient of the medium inside and outside of the elastic shell were investigated. Our findings led to the following conclusions.

(i) In the high-frequency acoustic field at 1 MHz, the main resonance response radius of the oscillating bubbles is approximately 2 μm, and the main resonance radius tends to decrease as the amplitude of the acoustic wave increases, indicating that increasing the amplitude of the acoustic wave at this frequency can drive smaller bubbles to resonate. The inhibitory effect of increasing the number of bubbles on bubble oscillation is strong when the number of bubbles exceeds 300 and the maximum dimensionless radius of the bubbles approaches 1.

(ii) The stress change in the elastic shell follows the opposite trend of bubble oscillation, reaching the maximum compressive and tensile stresses at the maximum radius of the bubble and at the time of bubble collapse, respectively, allowing the change in stress in the elastic shell to be predicted using the bubble oscillation curve.

(iii) Under high-frequency acoustic stimulation, the inertial cavitation threshold for bubbles around the initial radius

1–4 μm is low and approaches a minimum at 2 μm, making inertial cavitation easy to induce. When the initial radius of the bubble cluster is greater than 4 μm, the inertial cavitation threshold increases in proportion to the driving frequency, number of bubbles, and initial radius. The thickness of the elastic shell, initial inner radius, and shear modulus and viscosity coefficients of the medium within and outside the shell have a more complicated effect on the inertial cavitation threshold.

(iv) The instability of oscillating bubbles within a bubble cluster in a liquid cavity wrapped by an elastic shell is primarily controlled by the frequency and amplitude of the driving acoustic wave, initial radius of the bubbles, initial radius of the bubble cluster, and bubble number density. The minimal instability driving the sound pressure threshold increases significantly as the initial radius of the inner elastic shell decreases.

Our model provides a theoretical basis for ultrasound medical diagnosis and treatment. It can be used to select parameters for perfluorocarbon droplets and appropriate driving acoustic wave frequency, amplitude, and so on, to avoid shell rupture and to modulate parameters to achieve stable nonspherical oscillations of bubbles and inertial cavitation. We will continue to improve the model by taking into account the impact of mass exchange both within and outside the bubble as well as heat transmission.

Acknowledgement

Project supported by the National Natural Science Foundation of China (Grant No. 12374441).

References

[1] Park S, Yoon H, Emelianov S and Aglyamov S 2017 *Jpn. J. Appl. Phys* **56** 07JF10
[2] Harmon J N, Hyde J E, Jensen D E, D'Cessare E C, Odarenko A A, Bruce M F and Khaing Z Z 2024 *Exp. Neurol.* **374** 114681
[3] Pellow C, Jafari Sojahrood A, Zhao X, Kolios M C, Exner A A and Goertz D E 2024 *ACS Nano* **18** 410
[4] Wu N, Cao Y, Liu Y, Zhou Y, He H, Tang R, Wan L, Wang C, Xiong X, Zhong L and Li P 2023 *Front. Bioeng. Biotechnol.* **11** 1173381
[5] Honari A and Sirsi S R 2023 *Pharmaceutics* **15** 170
[6] Ho Y J, Huang C C, Fan C H, Liu H L and Yeh C K 2021 *Cell. Mol. Life Sci.* **78** 6119
[7] Li Q and Du L N 2021 *Acta Pharm Sin.* **56** 761
[8] Elhelf I A S, Albahar H, Shah U, Oto A, Cressman E and Almekkawy M 2018 *Diagn. Interv. Imaging* **99** 349
[9] Chen Y H, Moore D, Lee C C and Su Y H 2023 *J. Neuro-Oncol.* **165** 53
[10] Schenk H J, Steppe K and Jansen S 2015 *Trends Plant Sci.* **20** 199
[11] Noblin X, Rojas N O, Westbrook J, Llorens C, Argentina M and Dumais J 2012 *Science* **335** 1322
[12] Marti D, Krüger Y, Fleitmann D, Frenz M and Rička J J 2012 *Fluid Phase Equilib. Zones* **4** 13
[13] Church C C 1995 *J. Acoust. Soc. Am.* **97** 1510
[14] Obreschkow D, Kobel P, Dorsaz N, de Bosset A, Nicollier C and Farhat M 2006 *Phys. Rev. Lett.* **97** 094502
[15] Fourest T, Laurens J M, Deletombe E, Dupas J and Arrigoni M 2015 *Thin-Walled Struct.* **86** 67
[16] Vincent O and Marmottant P 2017 *J. Fluid Mech.* **827** 194
[17] Vincent O, Marmottant P, Gonzalez-Avila S R, Ando K and Ohl C D 2014 *Soft Matter* **10** 1455
[18] Wang Q X 2017 *Phys. Fluids* **29** 072101
[19] Gaudron R, Murakami K and Johnsen E 2020 *J. Mech. Phys. Solids* **143** 104047
[20] Qamar A, Wong Z Z, Fowlkes J B and Bull J L 2010 *Appl. Phys. Lett.* **96** 143702
[21] Gubaidullin D A and Fedorov Y Y 2020 *J. Appl. Mech. Tech. Phys.* **61** 517
[22] Yasui K, Iida Y, Tuziuti T, Kozuka T and Towata A 2008 *Phys. Rev. E* **77** 016609
[23] An Y 2011 *Phys. Rev. E* **83** 066313
[24] Shen X, Wu P and Lin W 2024 *Ultrason. Sonochem.* **107** 106890
[25] Huang C Y, Li F, Feng S Y, Wang C H, Chen S, Hu J, He X R and Song J K 2024 *Chin. Phys. B* **33** 024301
[26] Xu L, Yao X R and Shen Y 2024 *Chin. Phys. B* **33** 044702
[27] Zhang T R, Mo R Y, Hu J, Chen S, Wang C H and Guo J Z 2021 *Acta Phys. Sin.* **70** 124301 (in Chinese)
[28] Fedorov Y V and Gubaidullina D D 2023 *Lobachevskii J. Math.* **44** 1600
[29] Wang C H, Mo R Y, Hu J and Chen S 2015 *Acta Phys. Sin.* **64** 234301 (in Chinese)
[30] Song X, Loskutova K, Chen H, Shen G and Grishenkov D 2021 *J. Acoust. Soc. Am.* **150** 1750
[31] Qin D, Zou Q Q, Li Z Y, Wang W, Wan M X and Feng Y 2021 *Acta Phys. Sin.* **70** 154701 (in Chinese)
[32] Shao W and Chen W 2015 *J. Appl. Phys.* **117** 024702
[33] Zilonova E, Solovchuk M and Sheu T W H 2019 *Phys. Rev. E* **99** 023109
[34] Zhang W and An Y 2013 *Phys. Rev. E* **87** 053023
[35] Wu Q, Gray M, Smith C A B, Bau L, Cleveland R O, Coussios C and Stride E 2024 *J. Acoust. Soc. Am.* **156** 3608
[36] Ma Y, Zhang G and Ma T 2022 *Ultrason. Sonochem.* **84** 105953